Effective material properties for shear-horizontal acoustic waves in fiber composites

Christophe Aristégui
Université Bordeaux 1; CNRS; UMR 5469, Laboratoire de Mécanique Physique, Talence, F-33405 France

Yves C. Angel
University of Lyon, Lyon, F-69003, France; University Lyon 1, Lyon, F-69003, France; and INSERM U556, Therapeutic Applications of Ultrasound Laboratory, Lyon, F-69424, France

(Received 26 January 2006; revised manuscript received 13 March 2007; published 14 May 2007)

The effective dynamic properties of composites made of elastic cylindrical fibers randomly distributed in another elastic solid can be evaluated with plane shear-horizontal acoustic waves. In this paper, it is shown that the effective mass density and the effective shear stiffness are complex valued and frequency dependent. Simple formulas are derived for these effective quantities. The low-frequency limit of these formulas is found to be in agreement with physical expectations. The derivation is based on the multiple-scattering approach of Waterman and Truell, where each cylinder of finite cross section is replaced with an equivalent line scatterer. Numerical results are presented for the effective mass density and effective shear stiffness for various values of frequency, cylinder concentration, and elastic properties of the cylinders and matrix.

DOI: 10.1103/PhysRevE.75.056607 PACS number(s): 43.20.+g, 43.35.+d

I. INTRODUCTION

Ultrasound techniques are used to investigate materials with internal microstructures, such as reinforced composites [1–3] and adhesive polymers [4], and their average response is measured. The response is propagative if the microstructure is not too dense, and diffusive otherwise, where the density of the microstructure is determined by the ratio of the elastic mean free path in the material to the dominant wavelength in the probing signal.

The averaging that is mentioned above takes place over the disorder of the microstructure, so that the probing signal "sees" an effectively *homogeneous* material. This is an equivalent material from the viewpoint of wave propagation. The part of the motion that resists disorder after averaging over all possible configurations of fibers is the coherent motion. It has been shown elsewhere that the coherent motion makes each composite appear as a dissipative material, and propagation is governed by a complex-valued effective wave number that is frequency dependent. The imaginary part of this wave number is the attenuation.

Models have been proposed to predict the phase velocity and attenuation of effective plane waves in two-phase media [2–8], and to predict their effective mass density and elastic stiffness [1,9–15]. In these models, expressions for the effective mass density are assumed *a priori* [2,6,16], or else the scope of the work is restricted to the low-frequency limit [10,14].

This raises the question of whether better models can be constructed by eliminating *a priori* assumptions. To illustrate our point, we consider here the multiple-scattering approach proposed by Waterman and Truell [5], which is known to be valid for dilute distributions of scatterers. These authors have predicted the effective wave number of the coherent wave in a semi-infinite material [17]. Their expression depends on the far-field scattering properties, in the forward and backward directions, of a single scatterer.

Using the framework of Waterman and Truell, we have determined analytically the system of coherent waves that propagate inside and outside a layer of finite thickness [7,8,18,19]. The lossless scatterers are distributed uniformly and randomly inside the layer and are embedded in an elastic material. Thus, energy dissipation is induced only by multiple scattering, and no anelastic attenuation is present. To obtain our results, we have made no continuity assumption on the "boundaries" of the layer. We have obtained for the effective wave number K the same expression as that of Waterman and Truell, who considered a semi-infinite region. In our case, K describes propagation inside a finite-width layer.

In this paper, we show that both the effective mass density ρ and the effective shear stiffness M corresponding to shear-horizontal (SH) plane waves can be determined without further assumptions beyond those already contained in the approach of Waterman and Truell. To determine ρ and M, we need two equations.

First, we assume that the effective stress-strain response of the equivalent material is identical in form to that of an elastic solid subjected to SH wave motions. This allows us to write the dispersion equation that relates ρ, M, K, and the angular frequency ω of a harmonic excitation.

The second relation is obtained by comparing the response of the layer containing scatterers [7,8,18,19] with that of a homogeneous layer. The latter is well known in acoustics. Comparing these two approaches, we are able to identify the effective acoustic impedance of the layer.

Background results are presented in Secs. II and III. The formulas for the effective mass density and effective shear stiffness corresponding to SH plane motions are established in Sec. IV. Using these formulas, we perform numerical calculations, which are presented in Figs. 2–5 and discussed in Sec. V. The low-frequency limits of the formulas for ρ and M are obtained in Sec. VI. Concluding remarks are collected in Sec. VII. In particular, we comment on the importance of our analytical results for the accuracy of experimental measurements.

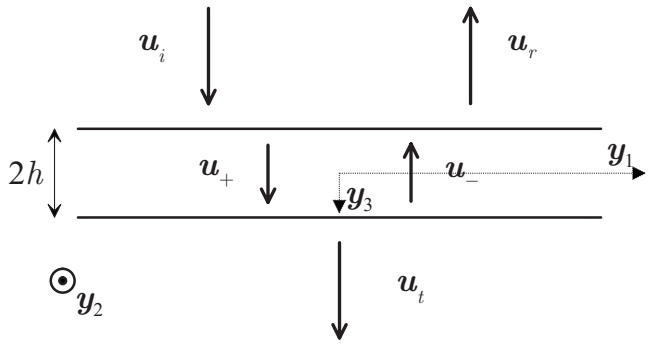

FIG. 1. Schematic diagram of SH waves propagating inside and outside a layer of thickness $2h$. The propagation vectors are in the y_3 direction. The particle displacements are in the y_2 direction.

II. PROBLEM STATEMENT

We consider a two-phase composite, where solid cylinders of radius a are distributed randomly and uniformly in a solid matrix that occupies the entire three-dimensional space. The cylinders and the matrix are made of linearly elastic and isotropic solids. Each cylinder has an axis of revolution that is parallel to the y_2 axis, as shown in Fig. 1.

Let a time-harmonic plane SH wave propagate in the matrix—without cylinders—along the y_3 direction. For simplicity, the time factor $e^{-i\omega t}$ will be omitted in the following. The displacement components associated with this wave have the form

$$u_1 = u_3 = 0, \quad u_2 = u_0 e^{ik_0 y_3}, \tag{1}$$

where $k_0 = \omega/c_0$ is the wave number, ω the angular frequency, c_0 the transverse wave speed in the matrix, and u_0 an amplitude factor.

When the wave (1) propagates in the cylinder-matrix composite, multiple scattering occurs. Then one observes either propagation or diffusion, or a combination of the two—depending on the frequency as well as on the geometrical and material properties of the composite [17].

Assuming that propagation occurs, one can describe the coherent wave motion in the composite by a complex-valued wave number K. This wave number has been evaluated analytically [20]. In the system of axes of Fig. 1, the coherent wave is represented by the displacement components

$$u_1 = u_3 = 0, \quad u_2 = A e^{iKy_3}, \tag{2}$$

where A is an amplitude factor.

In Eq. (1), the displacement component u_2 satisfies the equation of motion

$$\rho_0 \frac{\partial^2 u_2}{\partial t^2} = \mu_0 \frac{\partial^2 u_2}{\partial y_3^2}, \tag{3}$$

where ρ_0 and $\mu_0 = \rho_0 c_0^2$ are, respectively, the mass density and the shear modulus of the matrix. In Eq. (2), K is the effective wave number that governs SH wave propagation in the cylinder-matrix composite. The equation of motion for the effective material, by analogy with (3), has the form

$$\rho \frac{\partial^2 u_2}{\partial t^2} = M \frac{\partial^2 u_2}{\partial y_3^2}, \tag{4}$$

where u_2 is the displacement component of the coherent wave in the y_2 direction, ρ the effective mass density, and M the effective shear stiffness. Substituting (2) into (4), one finds that

$$\frac{\rho\omega^2}{K^2} = M. \tag{5}$$

Observe that M relates linearly the effective stress component σ_{23} to the effective strain component $e_{23} = \partial u_2/\partial y_3$. In the dispersion equation (5), ω and K are known. Thus, ρ and M are two unknowns. Next, we determine these two unknowns.

III. COMPOSITE LAYER

We consider a slab of thickness $2h$ made of the cylinder-matrix composite of Sec. II. The layer occupies the region of space $|y_3| < h$, as shown in Fig. 1. The regions $y_3 > h$ and $y_3 < -h$ outside the layer are occupied by the matrix only. We denote by n_0 the number of cylindrical cross sections per unit area in the plane of the figure. Each cylinder is represented as an equivalent anisotropic linelike scatterer that lies in the y_2 direction.

When the plane SH wave of Eq. (1) is normally incident on the layer, one finds that a system of plane SH coherent waves propagate in the entire space. Because of the translational invariance of the geometry and excitation, the coherent displacement has one component in the y_2 direction, which is given by

$$u_2(y_3) = \begin{cases} u_0 e^{ik_0 y_3} + u_0 R e^{-ik_0 y_3}, & y_3 < -h, \quad (6) \\ u_0 A_+ e^{iKy_3} + u_0 A_- e^{-iKy_3}, & |y_3| < h, \quad (7) \\ u_0 T e^{ik_0 y_3}, & y_3 > h. \quad (8) \end{cases}$$

Equations (6)–(8) show that a wave of amplitude R is reflected into the region $y_3 < -h$, and a wave of amplitude T is transmitted into the other side of the layer, where $y_3 > h$. Inside the layer, two waves of amplitudes A_- and A_+, respectively, propagate in the backward and forward directions. We have found, by using the approach of Waterman and Truell without further assumptions, that [8,18,19]

$$R = \frac{Qe^{-2ik_0 h}}{1 - Q^2 e^{4iKh}}(1 - e^{4iKh}), \tag{9}$$

$$T = \frac{1 - Q^2}{1 - Q^2 e^{4iKh}} e^{2i(K - k_0)h}, \tag{10}$$

$$A_- = -\frac{Q(1+Q)}{1 - Q^2 e^{4iKh}} e^{i(3K - k_0)h}, \tag{11}$$

$$A_+ = \frac{1+Q}{1 - Q^2 e^{4iKh}} e^{i(K - k_0)h}. \tag{12}$$

In Eqs. (9)–(12), one has

$$K^2 = k_0^2\left(1 + n_0\frac{2\pi}{k_0^2}f(0)\right)^2 - k_0^2\left(n_0\frac{2\pi}{k_0^2}f(\pi)\right)^2, \quad (13)$$

$$Q = \frac{1-\Theta}{1+\Theta}. \quad (14)$$

The quantity Θ in (14) is defined by

$$\Theta = \frac{k_0}{K}\left(1 + \frac{2\pi n_0}{k_0^2}[f(0)+f(\pi)]\right) = \frac{K}{k_0}\left(1 + \frac{2\pi n_0}{k_0^2}[f(0)-f(\pi)]\right)^{-1}. \quad (15)$$

In Eqs. (13) and (15), $f(0)$ and $f(\pi)$ stand for the far-field amplitudes scattered by a single cylinder in the forward ($\theta=0$) and backward ($\theta=\pi$) directions, respectively.

The results (9)–(15) are obtained as direct consequences of the Waterman and Truell approach for multiple scattering [5]. In that approach, no assumptions are made concerning the effective mass density and shear stiffness of the cylinder-matrix composite. Nor are continuity conditions written on the "interfaces" $y_3=\pm h$ between the layer and the matrix.

Next, we consider a homogenous layer made of a linearly elastic solid with isotropy properties in the (y_1,y_3) plane and mass density ρ_h. Let the layer occupy the region $|y_3|<h$ of Fig. 1 between two half spaces of the matrix material. Then, when the time-harmonic plane SH wave of Eq. (1) is incident on the layer, one finds a system of plane waves as in Eqs. (6)–(12), provided that the factor Q and the effective wave number K be replaced, respectively, with

$$Q = \left(1 - \frac{\rho_h k_0}{\rho_0 k_h}\right) \Big/ \left(1 + \frac{\rho_h k_0}{\rho_0 k_h}\right), \quad K = k_h, \quad (16)$$

where k_h is the wave number inside the homogeneous layer.

The results (9)–(12), combined with (16), are well known in acoustics. They are obtained by writing continuity of displacement and shear stress at the interfaces $y_3=\pm h$. We observe that $\rho_h k_0/\rho_0 k_h$ is the ratio of the acoustic impedance of the homogeneous layer to that of the lossless surrounding solid.

IV. EFFECTIVE MASS DENSITY AND SHEAR STIFFNESS

In view of the preceding discussion, we define the effective solid corresponding to the cylinder-matrix composite as follows. It is the homogeneous solid of mass density ρ where coherent SH waves propagate with the wave number K of Eq. (13). Thus, we infer from (14) and (16) that

$$\frac{\rho k_0}{\rho_0 K} = \Theta, \quad (17)$$

where Θ is given by (15). It follows from (15) and (17) that

$$\rho = \rho_0\left(1 + \frac{2\pi n_0}{k_0^2}[f(0)+f(\pi)]\right). \quad (18)$$

Then, substituting (13) and (18) into the dispersion equation (5), one finds that

$$M = \mu_0\left(1 + \frac{2\pi n_0}{k_0^2}[f(0)-f(\pi)]\right)^{-1}. \quad (19)$$

Equations (18) and (19) are the main results of this paper. Since the far-field scattering amplitude $f(\theta)$ is complex valued in general, we infer from (18) and (19), respectively, that the effective mass density and the effective shear stiffness are complex valued. Both are also frequency dependent.

We recall that complex-valued mass densities are used to represent wave propagation in porous media [21], and complex-valued stiffnesses are associated with wave attenuation in viscoelastic solids.

Isotropic scattering corresponds to the particular situation where the amplitude of the far-field motion scattered by each cylinder is constant in all directions. Thus, one has $f(0)=f(\pi)$ [8,22], and it follows from (19) that

$$M = \mu_0. \quad (20)$$

Equation (20) shows that the shear stiffness of the composite is equal to that of the matrix for isotropic scattering.

V. CYLINDRICAL CAVITIES AND FIBERS

In this section, we present numerical results corresponding to the effective mass density given by (18) and to the effective shear stiffness given by (19). We consider first the case of empty cylindrical cavities and then the case of cylindrical fibers made of an isotropic linearly elastic solid. In either case, the matrix is made of an isotropic linearly elastic solid. The mass densities, shear moduli, and transverse sound speeds of the matrix and fibers, respectively, are denoted ρ_0,μ_0,c_0 and ρ_1,μ_1,c_1. The empty cylindrical cavities can be viewed as fibers of mass density $\rho_1=0$ and shear modulus $\mu_1=0$.

We recall that the far-field scattering amplitude $f(\theta)$ corresponding to a plane time-harmonic SH wave of frequency ω incident on a cylindrical scatterer is given by

$$f(\theta) = \frac{1}{i\pi}\sum_{n=0}^{+\infty}\varepsilon_n C_n \cos(n\theta). \quad (21)$$

In Eq. (21), the angle θ is measured from the positive y_3 direction of Fig. 1, and ε_n denotes the Neumann factor, which is such that $\varepsilon_0=1$ and $\varepsilon_n=2$ for $n\geqslant 1$.

The coefficients C_n describe the scattering properties of the cylinder. They depend on the frequency and cylinder radius, as well as on the material properties of the cylinder and those of the surrounding solid. To evaluate these coefficients, we write continuity conditions on the cylinder surface. The stress component σ_{23} is continuous, and so is the displacement component u_2 (in the case of a solid cylinder). When the scatterer is a cylindrical cavity, the displacement u_2 on the cavity surface is not subjected to a continuity condition.

The scattering coefficients C_n corresponding to SH waves are given in the Appendix in terms of the dimensionless frequency

$$\tilde{\omega} = k_0 a. \quad (22)$$

Figure 2 shows the real and imaginary parts of ρ/ρ_0 in a solid containing empty cylindrical cavities. The frequency $\tilde{\omega}$

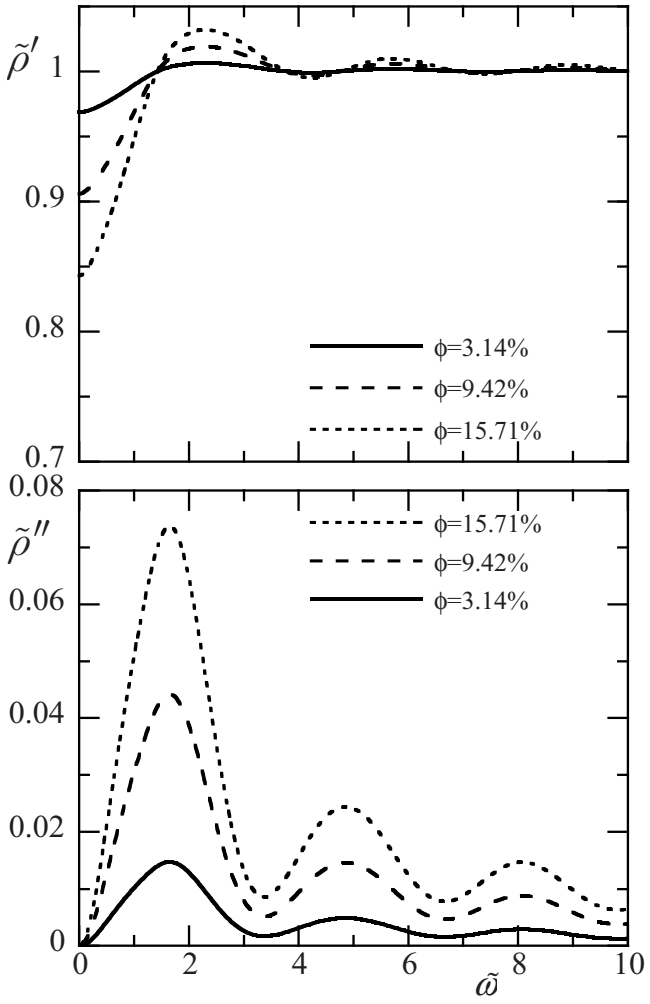

FIG. 2. Real and imaginary parts of the effective mass density ρ/ρ_0 $(=\tilde{\rho}'+i\tilde{\rho}'')$ for empty cylindrical cavities in an elastic solid versus the dimensionless frequency $\tilde{\omega}$ for three concentrations ϕ.

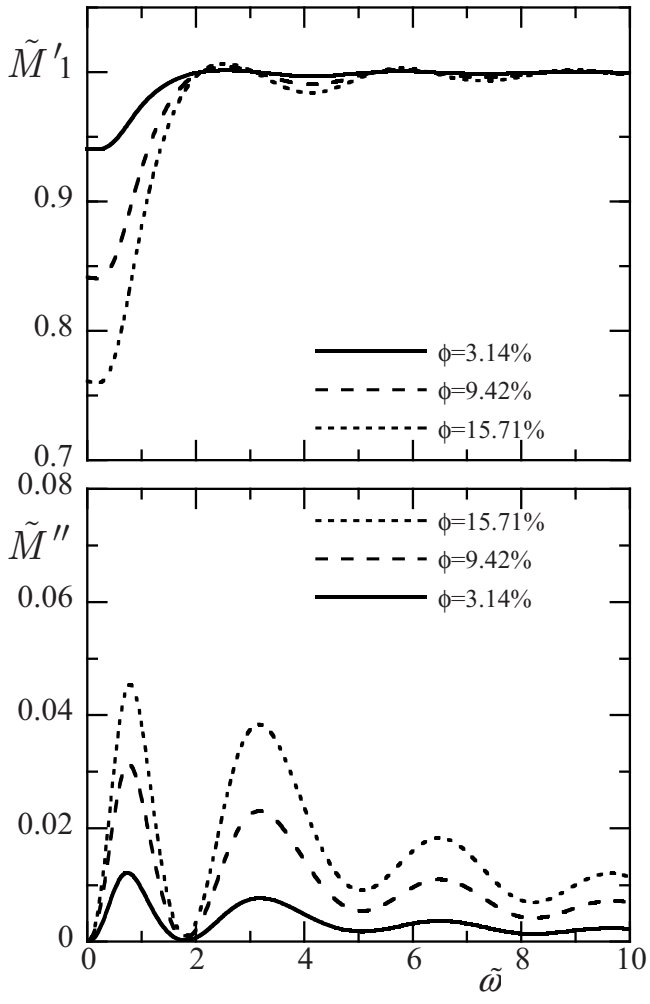

FIG. 3. Real and imaginary parts of the effective shear stiffness M/μ_0 $(=\tilde{M}'-i\tilde{M}'')$ for empty cylindrical cavities in an elastic solid versus the dimensionless frequency $\tilde{\omega}$ for three concentrations ϕ.

varies from 0 to 10 along the horizontal axis, which means that the incident wavelength $\lambda_0=2\pi/k_0$ takes values between approximately $0.6a$ and ∞.

The curves in Fig. 2 correspond to three values of the surface concentration $\phi=n_0a^2\pi=3.14\%$, 9.42%, and 15.71%. We observe that, for a close-packed cylinder arrangement, the concentration ϕ is equal to $\pi/4$, which gives a percentage value of 78.5%.

The imaginary part of ρ/ρ_0 takes values less than 0.08, and is much smaller than the real part, which is close to unity. We see that the two curves display cyclic variations with maxima and minima that are independent of ϕ. When ϕ increases, $\mathrm{Im}(\rho/\rho_0)$ increases for each given value of $\tilde{\omega}$, and $\mathrm{Re}(\rho/\rho_0)$ decreases in the range $0<\tilde{\omega}<1.5$ approximately.

Beyond $\tilde{\omega}\simeq 1.5$, the real part of ρ/ρ_0 oscillates and, at some frequencies, takes values that are greater than 1. At those frequencies, the solid containing holes appears heavier than the solid without holes. This is an unexpected result, which suggests that the holes behave as though they were filled with a solid of mass density higher than ρ_0. Alternatively, the solid matrix behaves as though it had a mass density higher than ρ_0.

If the curves of Fig. 2 were continued beyond $\tilde{\omega}=10$, toward higher frequencies, it appears that $\mathrm{Re}(\rho/\rho_0)$ would approach 1 and $\mathrm{Im}(\rho/\rho_0)$ would approach zero. Thus, in this limit, the effective mass density is that of the solid matrix.

Figure 3 shows the real and imaginary parts of M/μ_0 in a solid containing empty cylindrical cavities. The frequency $\tilde{\omega}$ and the concentration ϕ are as in Fig. 2.

The imaginary part of M/μ_0 takes values less than 0.05, and the real part of M/μ_0 varies between 0.75 and 1. The two curves display cyclic variations. There are some frequencies at which $\mathrm{Re}(M/\mu_0)$ is greater than 1, which indicates that the solid with holes can be stiffer than the solid without holes.

Figure 4 shows the real and imaginary parts of ρ/ρ_0 in a solid containing elastic fibers. The frequency $\tilde{\omega}$ varies on the horizontal axis as in Figs. 2 and 3. The concentration ϕ is fixed and equal to 15.71%. Each curve corresponds to a fixed value of the ratio $\mu=\mu_1/\mu_0$, which is also equal to $\rho_1c_1^2/\rho_0c_0^2$. Values of μ in the figure are 0.25, 0.5, 2/3, 1.5, 2, and 4. To simplify this parametric study, the transverse speeds have been chosen such that $c_0=c_1$. The figure is intended to illustrate the variations of $\mathrm{Re}(\rho/\rho_0)$ and those of

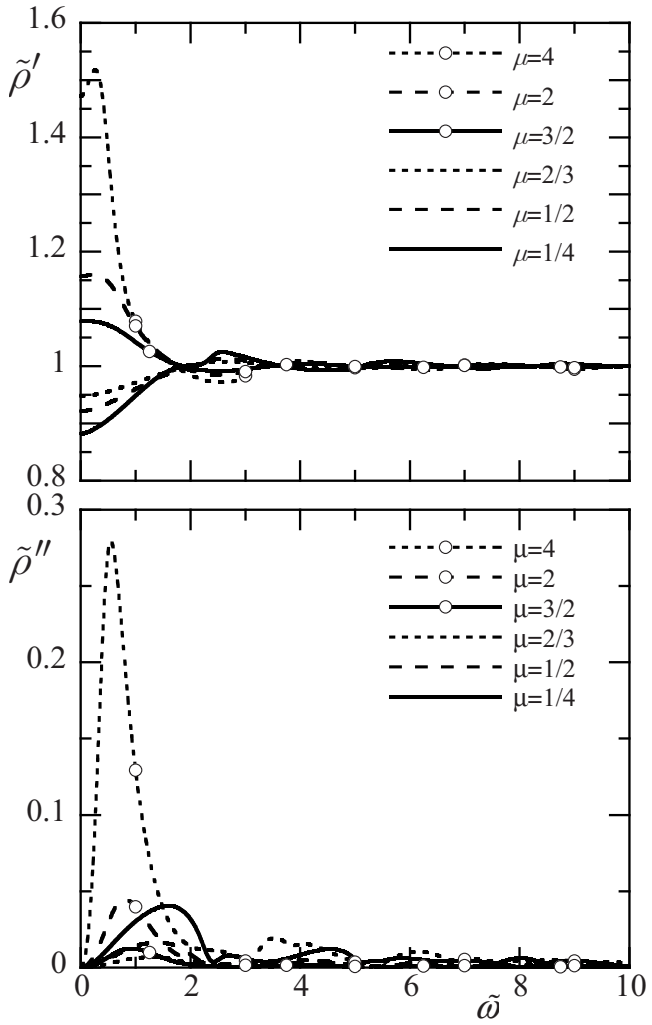

FIG. 4. Real and imaginary parts of the effective mass density ρ/ρ_0 $(=\tilde{\rho}'+i\tilde{\rho}'')$ for elastic circular cylinders in elastic solids versus the dimensionless frequency $\tilde{\omega}$ for various stiffness ratios μ. $\phi=15.71\%$ and $c_0=c_1$.

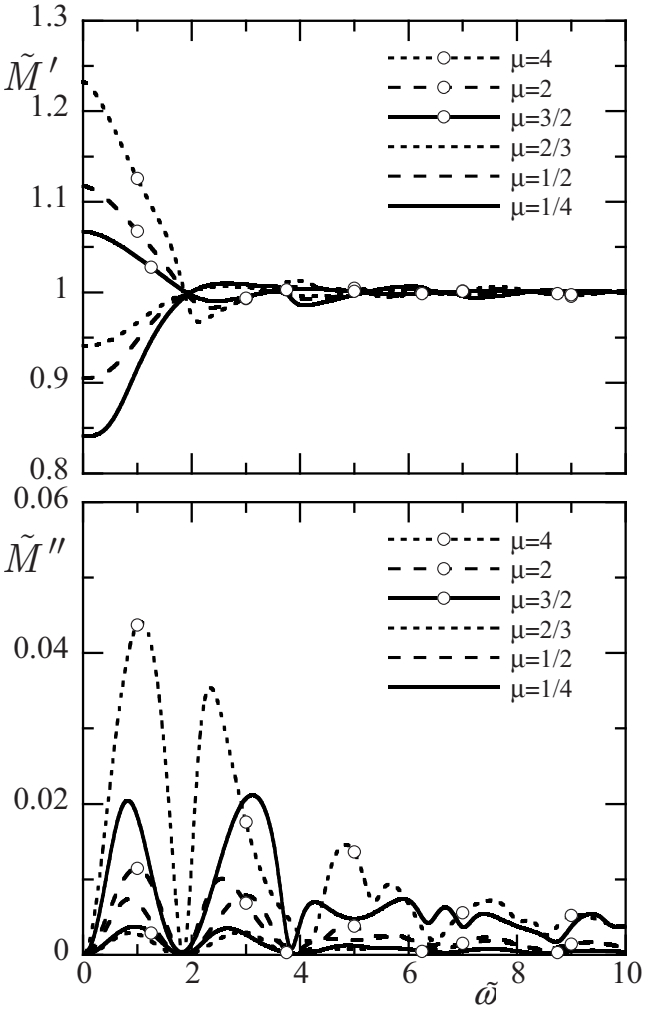

FIG. 5. Real and imaginary parts of the effective shear stiffness M/μ_0 $(=\tilde{M}'-i\tilde{M}'')$ for elastic circular cylinders in elastic solids versus the dimensionless frequency $\tilde{\omega}$ for various stiffness ratios μ. $\phi=15.71\%$ and $c_0=c_1$.

$\mathrm{Im}(\rho/\rho_0)$ in terms of the parameter μ when the speeds c_0 and c_1 are close. For example, if we take a steel matrix and aluminum fibers, then we find $\mu=0.31$. With an aluminum matrix and steel fibers, we find $\mu=3.19$. Observe that the transverse speeds in steel and aluminum are close to 3200 m/s. We see that, for $\tilde{\omega}$ greater than 2, $\mathrm{Re}(\rho/\rho_0)$ and $\mathrm{Im}(\rho/\rho_0)$ are rather insensitive to variations of μ. $\mathrm{Im}(\rho/\rho_0)$ approaches 0.3 at $\tilde{\omega}\simeq 0.6$ for the highest value of μ $(\mu=4)$. We observe also that $\mathrm{Re}(\rho/\rho_0)$ becomes larger than 1 at low frequencies $\tilde{\omega}$ when μ increases past 1. This is an expected result from a static point of view. It is not expected, however, that, at frequencies $\tilde{\omega}$ greater than 2, $\mathrm{Re}(\rho/\rho_0)$ becomes larger than 1 for values of μ less than 1. Indeed, in these circumstances, the fibers are lighter than the matrix.

Figure 5 shows the real and imaginary parts of M/μ_0 in a solid containing elastic fibers. The frequency $\tilde{\omega}$, the concentration ϕ, and the ratio μ are as in Fig. 4. $\mathrm{Im}(M/\mu_0)$ is less than 0.05 for all values of $\tilde{\omega}$ and μ.

At low frequency, $\mathrm{Re}(M/\mu_0)$ increases with μ and becomes greater than 1 when μ increases past 1. $\mathrm{Im}(M/\mu_0)$ vanishes in the limit of low frequency for all values of μ. For values of $\tilde{\omega}$ greater than 2, $\mathrm{Re}(M/\mu_0)$ is rather insensitive to variations of μ, and oscillates around 1. We find values of $\mathrm{Re}(M/\mu_0)$ greater than 1, even when μ is less than 1. Conversely, we find values of $\mathrm{Re}(M/\mu_0)$ less than 1, even when μ is greater than 1.

If the curves were continued past $\tilde{\omega}=10$, it appears that $\mathrm{Re}(M/\mu_0)$ would approach 1 and $\mathrm{Im}(M/\mu_0)$ would approach zero. This would be true for all values of μ. Thus, at high frequency, the stiffness of the composite approaches that of the matrix.

VI. LOW-FREQUENCY LIMIT

We find here the low-frequency limit of the effective mass density of Eq. (18) and that of the effective shear stiffness of Eq. (19). In the limit as $\tilde{\omega}$ approaches zero, the scattering coefficients C_n given in (A3) are such that

$$C_0(\tilde{\omega}) = i\frac{\pi}{4}\left(\frac{\rho_1}{\rho_0}-1\right)\tilde{\omega}^2 + O(\tilde{\omega}^4), \tag{23}$$

$$C_1(\tilde{\omega}) = i\frac{\pi}{4}\left(\frac{\mu_0 - \mu_1}{\mu_0 + \mu_1}\right)\tilde{\omega}^2 + O(\tilde{\omega}^4), \tag{24}$$

$$C_j(\tilde{\omega}) = O(\tilde{\omega}^4), \quad j \geqslant 2. \tag{25}$$

Then, using (23)–(25), one infers from (18) and (21) that the effective mass density ρ has the form

$$\rho = \rho_0 + \phi(\rho_1 - \rho_0) \quad (\tilde{\omega} \to 0). \tag{26}$$

Equation (26) shows that in the static limit the effective mass density satisfies the mixture rule.

Next, using (23)–(25), one infers from (19) and (21) that the effective shear stiffness has the form

$$M = \frac{\mu_0}{1 + 2\phi\left(\frac{\mu_0 - \mu_1}{\mu_0 + \mu_1}\right)} \quad (\tilde{\omega} \to 0). \tag{27}$$

For empty cylindrical cavities, where $\rho_1 = 0$ and $\mu_1 = 0$, one finds that

$$\rho = (1 - \phi)\rho_0 \quad (\tilde{\omega} \to 0), \tag{28}$$

$$M = \frac{\mu_0}{1 + 2\phi} \quad (\tilde{\omega} \to 0). \tag{29}$$

Equations (26) and (27) show that ρ and M are real valued in the static limit, as expected. Equation (27) shows that M is greater than μ_0 when $\mu_1 > \mu_0$, less than μ_0 when $\mu_1 < \mu_0$, and equal to μ_0 when $\mu_1 = \mu_0$. In the particular case of empty cavities, we see from (28) and (29), respectively, that ρ and M decrease when the concentration ϕ increases. These results are expected on physical grounds.

Using the simple scattering approach proposed by Kuster and Toksöz [10]—as opposed to the multiple-scattering approach of this paper—we find that the effective stiffness in the low-frequency limit is given by

$$M = \mu_0 \frac{(\mu_0 + \mu_1) - \phi(\mu_0 - \mu_1)}{(\mu_0 + \mu_1) + \phi(\mu_0 - \mu_1)} \quad (\tilde{\omega} \to 0). \tag{30}$$

The result (30) is identical to that obtained on the basis of the composite cylinder assemblage model [23,24].

Using a self-consistent scheme [13], one finds that the low-frequency limit of the effective stiffness is given by

$$M = \frac{\mu_0}{2}\{1 - \mu + 2\phi(\mu - 1) + \sqrt{4\mu + [1 - \mu + 2\phi(\mu - 1)]^2}\} \quad (\tilde{\omega} \to 0), \tag{31}$$

where $\mu = \mu_1/\mu_0$. We note that in Eq. (27) of Ref. [13], the quantity $2\mu_2$ on the right-hand side should be replaced with μ_2.

In the dilute case ($\phi \ll 1$), all three formulas (27), (30), and (31) are identical to within terms of $O(\phi^2)$. The result is

$$\frac{M}{\mu_0} = 1 - 2\left(\frac{\mu_0 - \mu_1}{\mu_0 + \mu_1}\right)\phi + O(\phi^2) \quad (\tilde{\omega} \to 0 \text{ and } \phi \to 0). \tag{32}$$

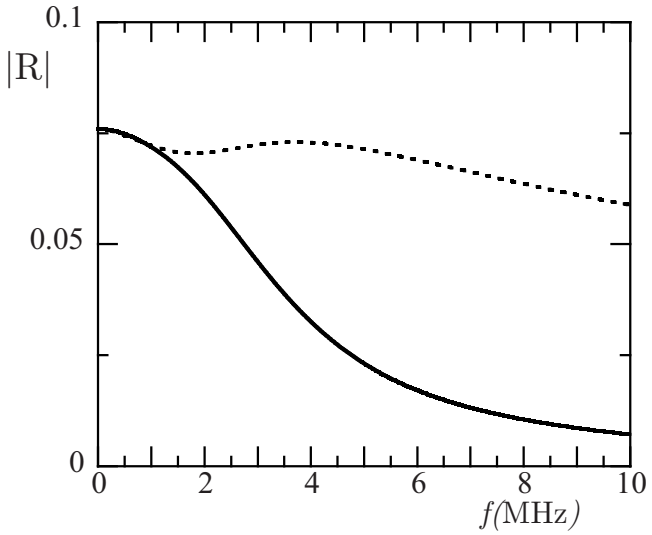

FIG. 6. Modulus of the reflection coefficient versus the frequency for a semi-infinite sample of a boron-epoxy composite. The radius and concentration of the boron fibers are 50 μm and 9.42%, respectively. The reflection coefficient is $R = -Q$, where Q is given by (14) and (17). In (17), $\Theta = \rho k_0/\rho_0 K$. Solid line: ρ is given by (18). Dashed line: ρ is given by the mixture law (26). $\rho_0 = 1261$ kg/m^3, $\rho_1 = 2682$ kg/m^3, $\mu_0 = 1.8$ GPa, and $\mu_1 = 161$ GPa.

In the case of isotropic scattering, all scattering coefficients in (21) must vanish, except C_0. Thus, in the low-frequency limit, we see from (23)–(25) that scattering is isotropic to within terms of $O(\tilde{\omega}^4)$ when $\mu_0 = \mu_1$. Then, from (27), $M = \mu_0$, which agrees with (20).

VII. CONCLUSION

Complex-valued frequency-dependent analytical formulas have been obtained for the effective mass density and effective shear stiffness of an elastic solid containing cylindrical fibers or cavities.

Our derivation is based on the multiple-scattering analysis of the problem proposed by Waterman and Truell. It yields formulas for the effective properties that depend on cylinder concentration and radius, and frequency, as well as on the forward and backward far-field scattered amplitudes corresponding to a single cylinder or cavity.

The formulas predict that the numerical values of the imaginary parts are much less than those of the real parts. The former should not be ignored, however, in an analysis of the multiple-scattering problem. For example, it would not be correct to assume that the effective mass density is real valued and given by the law of mixture at any frequency. Only in the low-frequency limit does the mass density formula reduce to that corresponding to the law of mixtures. Also, our formula for the shear stiffness agrees with those obtained elsewhere, in the low-frequency and low-scatterer-concentration limits.

Figure 6 illustrates the importance of using a complex-valued frequency-dependent mass density as in (18). This figure represents the modulus of the reflection coefficient for an epoxy matrix and boron fibers of concentration ϕ

=9.42%. The boron fibers are distributed in a semi-infinite space. In Fig. 6, the solid line is obtained by using the mass density (18), and the dashed line by using the mass density (26). We see that the two curves differ greatly from each other. This suggests to us that serious errors can result from using inappropriate expressions to model the effective mass density in experimental approaches.

Comparing our Eqs.(18) and (19), corresponding to SH waves, to those of Ref. [15], where P wave motions are investigated, we see that the effective material properties depend on the type of excitation. In each case, one has to solve a new multiple-scattering problem in order to infer the effective properties.

The effective acoustic impedance Z $(=\rho\omega/K)$ can be derived from (13) and (18). With Z, one can describe wave propagation inside and outside the two-phase layer of Fig. 1 by keeping track of the successive internal reflections on the boundaries of the equivalent homogeneous layer. There is an infinite number of reflections, which yields the reflection and transmission coefficients in the form of two infinite series. It is easy to interpret physically each term in the series. The two series converge, respectively, to the expressions (9) and (10), together with (13), (14), and (17). In electromagnetism, this is known as the Fabry-Pérot effect.

With the results of this paper, one can envision an approach to determine experimentally the phase velocity c and attenuation α of the coherent wave propagating inside a plate with internal microstructures. This is a problem of practical interest. We recall here that the reflection R and transmission T in (9) and (10) depend on two complex-valued quantities: the effective wave number $K=\omega/c+i\alpha$ and the effective mass density ρ. Thus, to determine c and α, one needs both R and T, unless one is willing to make an *a priori* assumption about the effective mass density.

APPENDIX: SCATTERING COEFFICIENTS

The scattering coefficients C_n for a single cylinder of radius a subjected to a SH wave are given in the following. The cylinder and the matrix are made of isotropic elastic solids. In the coordinate system of Fig. 1, the particle displacements are

$$\boldsymbol{u}_0(r,\theta,\omega)=\begin{cases}\left(\sum_{n=0}^{\infty}\varepsilon_n A_n J_n(k_0 r)\cos(n\theta)+\sum_{n=0}^{\infty}\varepsilon_n A_n C_n H_n^{(1)}(k_0 r)\cos(n\theta)\right)\boldsymbol{y}_2 & (r>a), \quad \text{(A1)}\\ \left(\sum_{n=0}^{\infty}\varepsilon_n A_n B_n J_n(k_1 r)\cos(n\theta)\right)\boldsymbol{y}_2 & (r<a), \quad \text{(A2)}\end{cases}$$

where $\boldsymbol{y}_2$ represents a unit vector in the y_2 direction, (r,θ) are the polar coordinates of the particle with origin located on the axis of the cylinder, and J_n and $H_n^{(1)}$ represent Bessel and Hankel functions of the first kind, respectively. The coefficients A_n are those in the Bessel expansion of the incident displacement of (1) and are given by $A_n=u_0 i^n$.

In Eq. (A1), the first term corresponds to the incident wave and the second term represents the scattered wave emanating from the cylinder. The coefficients A_n, A_nB_n, and A_nC_n represent amplitude factors. Imposing continuity of shear stress and out-of-plane displacement on the boundary of the cylinder of radius a, we find that the scattering coefficients have the form

$$C_n=-\frac{J_n\left(\frac{\tilde{\omega}}{\kappa}\right)[J_{n-1}(\tilde{\omega})-J_{n+1}(\tilde{\omega})]-\frac{\rho_1}{\rho_0}\kappa J_n(\tilde{\omega})\left[J_{n-1}\left(\frac{\tilde{\omega}}{\kappa}\right)-J_{n+1}\left(\frac{\tilde{\omega}}{\kappa}\right)\right]}{J_n\left(\frac{\tilde{\omega}}{\kappa}\right)[H_{n-1}^{(1)}(\tilde{\omega})-H_{n+1}^{(1)}(\tilde{\omega})]-\frac{\rho_1}{\rho_0}\kappa H_n^{(1)}(\tilde{\omega})\left[J_{n-1}\left(\frac{\tilde{\omega}}{\kappa}\right)-J_{n+1}\left(\frac{\tilde{\omega}}{\kappa}\right)\right]}. \quad \text{(A3)}$$

In Eq. (A3), one has $\tilde{\omega}=k_0 a$ and $\kappa=c_1/c_0$.

In the case of an empty cylindrical cavity, the coefficients C_n are also given by Eq. (A3), where $\rho_1=0$. Observe that, with $\rho_1=0$ in (A3), the J_n terms cancel out in the numerator and denominator. One finds the same answer by solving the cavity problem, with no boundary condition imposed on the displacement.

[1] J.-Y. Kim, J. Acoust. Soc. Am. **113**, 2442 (2003).
[2] V. K. Varadan, V. V. Varadan, and Y.-H. Pao, J. Acoust. Soc. Am. **63**, 1310 (1978).
[3] X. D. Wang and S. Gan, J. Appl. Mech. **69**, 696 (2002).
[4] R. E. Challis, R. P. Cocker, and A. K. Holmes, Ultrasonics **34**, 355 (1996).
[5] P. C. Waterman and R. Truell, J. Math. Phys. **2**, 512 (1961).
[6] L. W. Anson and R. C. Chivers, J. Phys. D **26**, 1566 (1993).
[7] Y. C. Angel and Y. K. Koba, Int. J. Solids Struct. **35**, 573 (1998).
[8] C. Aristégui and Y. C. Angel, Wave Motion **36**, 383 (2002).
[9] V. Twersky, J. Acoust. Soc. Am. **36**, 1314 (1964).
[10] G. T. Kuster and M. N. Toksöz, Geophysics **39**, 587 (1974).
[11] J. G. Berryman, J. Acoust. Soc. Am. **68**, 1809 (1980).

[12] R. L. Kligman, W. M. Madigosky, and J. R. Barlow, J. Acoust. Soc. Am. **70**, 1437 (1981).
[13] J.-Y. Kim, J. Acoust. Soc. Am. **100**, 2002 (1996).
[14] J. Li and C. T. Chan, Phys. Rev. E **70**, 055602(R) (2004).
[15] C. Aristégui and Y. C. Angel, Wave Motion **44**, 153 (2007).
[16] S. K. Bose and A. K. Mal, Int. J. Solids Struct. **9**, 1075 (1973).
[17] A. Derode, A. Tourin, and M. Fink, Phys. Rev. E **64**, 036605 (2001).
[18] Y. C. Angel, C. Aristégui, and J.-Y. Chapelon, in *Proceedings of the Second Biot Conference on Poromechanics, 2002*, edited by J.-L. Auriault, C. Geindreau, P. Royer, J.-F. Bloch, C. Boutin, and L. Lewandowska (AA Balkema, Rotterdam, 2002), p. 607.
[19] Y. C. Angel and C. Aristégui, J. Acoust. Soc. Am. **118**, 72 (2005).
[20] C. M. Linton and P. A. Martin, J. Acoust. Soc. Am. **117**, 3413 (2005).
[21] V. Tournat, V. Pagneux, D. Lafarge *et al.*, Phys. Rev. E **70**, 026609 (2004).
[22] L. L. Foldy, Phys. Rev. **67**, 107 (1945).
[23] Z. Hashin and B. W. Rosen, J. Appl. Mech. **31**, 223 (1964).
[24] R. M. Christensen, *Mechanics of Composite Materials* (Wiley, New York, 1979).